JAAS

ROYAL SOCIETY OF CHEMISTRY

TECHNICAL NOTE

View Article Online
View Journal | View Issue

Cite this: *J. Anal. At. Spectrom.*, 2021, **36**, 1374

Optimization of irradiation parameters for $^{40}Ar/^{39}Ar$ dating by Argus VI multi-collector mass spectrometry†

Wan-Feng Zhang, *[abce] De-Wen Zheng,[ab] Guo-Qing Liu, *[d] Yi-Gang Xu[abce] and Ying-De Jiang[ab]

Received 14th February 2021
Accepted 26th April 2021

DOI: 10.1039/d1ja00055a

rsc.li/jaas

In $^{40}Ar/^{39}Ar$ dating, $^{39}Ar_K$ generated is dependent on irradiation conditions, and the accumulation fast neutron fluence is a critical parameter for $^{40}Ar/^{39}Ar$ dating. With technological advancement, especially in the ultra-low background and multicollector technology, the boundary conditions to choose irradiation conditions have been greatly improved. Based on the detected and processed signal, the maximum boundary condition of $^{40}Ar^*/^{39}Ar$ can be up to 5750, meaning that very low ^{39}Ar signals can yield considerable analytical accuracy. In this study, one biotite sample (ZBH-25) was irradiated for 4 hours to assess the modified irradiation conditions, and the high $^{40}Ar^*/^{39}Ar$ ratio up to 4100 could yield ~1% analytical uncertainty. This reveals that the new boundary condition is useful to choose fast neutron fluence, especially for very old or low K/Ca ratio samples.

1. Introduction

$^{40}Ar/^{39}Ar$ dating is one of the most widely used geochronological and thermochronological techniques.[1,2] The released argon from the neutron-irradiated sample provides age information. The potassium content of a sample is indirectly determined by measuring ^{39}Ar, which is produced by the $^{39}K(n,p)^{39}Ar$ reaction during neutron irradiation. Thus, the irradiation step is a critical step before $^{40}Ar/^{39}Ar$ analysis. The choice of an optimum integrated neutron flux has a number of prerequisites, including sufficient ^{39}Ar produced from ^{39}K (which allows accurate age determination) and minimal ^{40}Ar and ^{36}Ar production (from $^{40}K(n,p)^{40}Ar$ and $^{40}Ca(n,n\alpha)^{36}Ar$, respectively).[3]

The optimum integrated neutron flux for a given rock sample is determined primarily by its age and K/Ca ratio. Based on the analytical ability and arbitrarily, Grenville Turner[3] proposed a convenient method to choose the accumulation fluence of fast neutrons based on $^{40}Ar^*/^{39}Ar = \sim 300$ and $K/Ca = \geq 0.01$ as the boundary conditions to yield acceptable analytical uncertainty (~1%). The maximum boundary conditions ($^{40}Ar^*/^{39}Ar$ ratio) for choosing the accumulation fluence of fast neutrons can be relaxed to ~1000 if the mass spectrometer has adequate resolution and a low background (especially for the background of ^{39}Ar). This method remains a sensible choice in single detector analytical technology, which requires a sufficient amount of Ar isotopes to yield precise results.[1] Such a requirement can be easily met when the samples are K-rich and Ca-poor. However, for Ca-rich and K-poor samples, such as plagioclase or mid-oceanic ridge basalt, it is hard to satisfy both sufficient ^{39}Ar production (from ^{39}K) and side effect reduction (by ^{40}Ca). As the sample size is chosen accordingly to yield an adequate amount of ^{40}Ar for the analysis, this does not allow the increase of the sample volume. Furthermore, the K/Ca ratio is constant in samples; relaxing the $^{40}Ar^*/^{39}Ar$ ratio is therefore a suitable choice to select the irradiation parameters. This method represents a reasonable guide to choose the irradiation conditions and to equilibrate the influence of the $^{40}Ca(n,n\alpha)^{36}Ar$ and $^{39}K(n,p)^{39}Ar$ reaction.

With the development of analytical technology, especially in laser step heating and the multi-collector technology, the detection limit has greatly reduced. Moreover, the reproducibility of $^{40}Ar/^{36}Ar$ in repeated air standards is approximately 5 times better than that of its counterpart from single-collector mass spectrometers in a peak-jumping mode.[4] These improvements allow better analysis for K-poor samples. The boundary conditions ($^{40}Ar^*/^{39}Ar = \sim 300$ and $K/Ca \geq 0.01$) set in previous studies[3] would need to be upgraded. Particularly the maximum of the $^{40}Ar^*/^{39}Ar$ ratio needs to be reconsidered when choosing the accumulation fast neutron flux during sample irradiation. Moreover, decreasing the cumulative fluence of fast neutrons

[a]State Key Laboratory of Isotope Geochemistry, Guangzhou Institute of Geochemistry, Chinese Academy of Sciences, Guangzhou 510640, China. E-mail: wfzhang@gig.ac.cn
[b]CAS Center for Excellence in Deep Earth Science, Guangzhou, 510640, China
[c]Southern Marine Science and Engineering Guangdong Laboratory (Guangzhou), Guangzhou 511458, China
[d]College of Physics and Optoelectronic Engineering, Shenzhen University, Shenzhen 518060, China. E-mail: liugq@szu.edu.cn
[e]College of Earth and Planetary Sciences, University of Chinese Academy of Sciences, Beijing 100049, China

† Electronic supplementary information (ESI) available. See DOI: 10.1039/d1ja00055a

during sample irradiation has the following advantages: (1) reduces the irradiation time; (2) reduces sample irradiation dose; (3) enables better choice of accumulation fast neutron flux for ultra-low K/Ca ratio samples. Here, we performed experiments to estimate the maximum acceptable $^{40}Ar/^{39}Ar$ ratio with Argus VI multi-collector mass spectrometry, and estimated the lower boundary for selecting the optimum irradiation parameters.

2. Analytical methods

2.1. Instrumentation

The Argus VI is an all-metal single focusing noble gas mass spectrometer, and is built specifically for simultaneous analysis of argon isotopes.[4] The Argus VI can achieve an ultra-low background and enhanced sensitivity, compared to single collector mass spectrometers. The multiple collector array comprises a fixed five Faraday array (H2, H1, Ax, L1 and L2) and a compact discrete dynode (CDD). This Faraday array contains new high-gain amplifier circuits that allow gains of 10^{10} to 10^{13} Ω measuring resistors to be used. The 10^{11} Ω amplifier circuits are installed on H2 and the other Faraday detectors use 10^{12} Ω amplifier circuits. The sample preparation system installed in the Guangzhou Institute of Geochemistry includes an air tank (22.4 L) with a pipette system (0.1 mL), an in-house mini efficient purification system (273 mL),[5] a diamond windowed chamber and a ZnS windowed chamber with a CO_2 laser (10.6 μm, 50 W), and an automatic degas system. The purification system contains a cryotrap and 2 getters: one maintained at 400 °C and the other at room temperature. An in-house automatic degassing system was developed to yield an ultra-low background (static increase rate of $^{40}Ar < 6.98 \times 10^{-13}$ ccSTP per min).[6]

2.2 Standard gas preparation

To evaluate the stability and mass discrimination factor (MDF) of our equipment, air was injected into the purification system through the air tank-pipette system using the below workflow (Fig. 1):

(1) Open P1 and wait for 60 s to pump the pipette, and then close P1;

(2) Open P2 and wait for 60 s, letting the air balance to the pipette;

(3) Close P2, P7 and P8, and then open P1 and wait for 60 s to balance the gas to the purification system. After that, close P1 and the sample S0 is prepared.

To estimate the analytical precision in different amounts of argon signals during the analysis, other sample types are produced by the following workflow. After the sample S0 prepared, close P3 and open P7, and pump for 120 s. After that close P7 and open P3, and then wait for 60 s to reach a new balance in the purification system, and the sample was named sample S1. The other seven kinds of samples can be prepared by looping the above workflow, and are hereby named S2 to S8. According to the cup configuration used in this study, we use cup H2 and L2 to measure ^{40}Ar and ^{36}Ar simultaneously. Despite CDD being more suitable for low signal analysis, this multicollector configuration is unsuitable for high $^{40}Ar/^{39}Ar$ ratios as both ^{40}Ar and ^{39}Ar are detected on the 10^{12} Ω circuit Faraday cup. Thus, the detection limit of the 10^{11} and 10^{12} Ω circuits was evaluated using 9 different ion beam samples (Sample S0 to S8). The average signal and all analysis results of the different sample types are shown in Table 1 and the Appendix, respectively.

2.3 $^{40}Ar/^{39}Ar$ dating

To verify the method to choose accumulation fluence of fast neutrons, the geological standard Fcs was co-irradiated with the ZBH-25 biotite geostandard (from Fangshan in SW Beijing, China, 132.7 ± 0.1 Ma),[7] which was analyzed as an unknown. A total of seven aliquots were packed in aluminum foil, including ZBH-25, FCT, K_2SO_4 and CaF_2, and then placed in a silica tube. The samples were irradiated in the Miniature Neutron Source Reactor (MNSR) installed in the Shenzhen University. The MNSR is a compact nuclear facility. The fast neutron fluence is $\sim 5.246 \times 10^{11}$ n cm^{-2} s^{-1}, and 10 mg of each sample was irradiated for 4 hours.

Prior to the experiment, the extraction and purification systems were backed by the in-house automatic degassing system to reduce the system blank.[6] The sample in the chamber was heated by a temperature-controlled furnace at 150 °C for 24 hours. In order to correct the system blanks, cool blanks were used at the start and the end of each sample measurements, and between every four to six steps of sample analyses. The samples were step-heated using a continuous wave CO_2 laser instrument (50 W). The released gas was firstly cleaned up

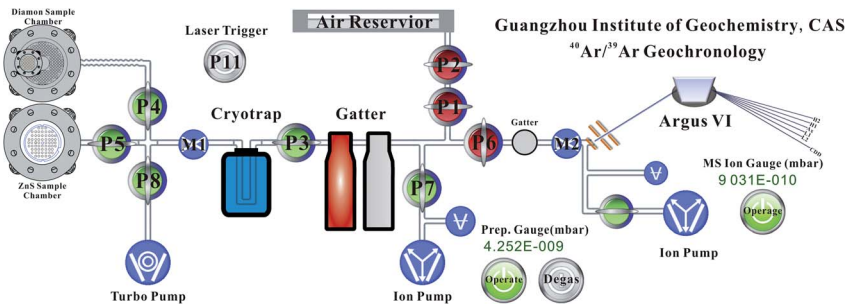

Fig. 1 Sketch of the Argus VI noble gas mass spectrometer in GIGCAS.

through a cryotrap (−100 °C), and then further purified using two SAES NP10 Zr/Al getters at ~400 °C and at room temperature, respectively, resulting in purified noble gases for argon isotope analyses in the mass spectrometer. The ^{40}Ar, ^{39}Ar, ^{38}Ar, ^{37}Ar, and ^{36}Ar isotope concentrations, extrapolated to time zero by linear fitting, were corrected for the background, mass discrimination, interfering isotope reactions, and ^{37}Ar decay since the time of irradiation. Mass discrimination of air from the automatic pipette system was assessed before analyzing the samples (^{40}Ar/^{36}Ar = 298.56).[8] The ^{40}Ar/^{39}Ar plateau ages and isochron ages were calculated using ArArCALC, Version 2.52.[9] The data reporting norms followed the approach described by Schaen *et al.*[10] Raw data, correction factors, ^{40}Ar/^{39}Ar age spectra, and isochron plots are presented in the Appendix.

3. Estimates of boundary conditions for irradiation neutron flux selection

3.1 Sufficiency of ^{39}Ar

For ^{40}Ar/^{39}Ar dating,[11,12] ^{39}Ar is generated from ^{39}K during irradiation with fast neutrons, and the sample age calculations can be expressed by eqn (1),

$$t = \frac{1}{\lambda}\ln\left(1 + J\frac{^{40}\mathrm{Ar}^*}{^{39}\mathrm{Ar_K}}\right) \quad (1)$$

$$\lambda = \lambda_{\beta-} + \lambda_e + \lambda'_e \quad (2)$$

$$J = \frac{^{39}\mathrm{K}}{^{40}\mathrm{K}}\frac{\lambda}{\lambda_e + \lambda'_e}\Delta t\int \Phi(E)\sigma(E)\mathrm{d}E \quad (3)$$

where t is the sample age (year). ^{40}Ar* is the radiogenic argon and ^{39}Ar$_K$ is the ^{39}Ar produced from ^{39}K during the irradiation. λ is the sum of decay constants for ^{40}K, including $\lambda_{\beta-}$, λ_e and λ'_e expressed in eqn (2). The decay constants of ^{40}K by β-emission and K-capture in 4.9737 (±0.0093) × 10^{-10} a^{-1},[13] 0.5755 (±0.0016) × 10^{-10} a^{-1},[13] and 0.0088 (±0.0017) × 10^{-10} a^{-1},[14] for $\lambda_{\beta-}$, λ_e and λ'_e, respectively. J is a dimensionless irradiation parameter defined by Crasty and Mitchell[12] and Mitchell,[15] as shown in eqn (3). Δt is the irradiation duration, $\Phi(E)$ is the neutron flux at energy (E), and $\sigma(E)$ is the neutron capture cross section at energy (E) for the ^{39}K(n,p)^{39}Ar reaction.

To estimate the lower boundary of the irradiation neutron flux, eqn (1) can be rearranged into eqn (4). Thus, for a given ^{40}Ar/^{39}Ar ratio, J is a function of t, meaning the analytical precision of ^{40}Ar/^{39}Ar limits the choice of accumulation fluence of fast neutrons (to be discussed in Section 4).

$$J \geq \frac{(e^{\lambda t} - 1)}{^{40}\mathrm{Ar}^*/^{39}\mathrm{Ar_K}} \quad (4)$$

3.2. ^{40}Ca(n,nα)^{36}Ar interference

^{36}Ar production by the neutron action on Ca in the sample is undesirable, and would interfere in the correction for atmospheric ^{40}Ar based on the sample ^{36}Ar content. In order to compare with the previous work with ≤1% uncertainty,[3] the interference from this source for ^{40}Ar*/^{36}Ar$_{Ca}$ needs to be ≥29 856, according to the latest proposed atmospheric ratio (normalized to atmospheric ^{40}Ar/^{36}Ar = 298.56).[8] Eqn (5) represents the K–Ar dating computational formula,[1,16] and can be rearranged into eqn (6).

$$t = \frac{1}{\lambda}\ln\left(1 + \frac{\lambda}{\lambda_e + \lambda'_e}\frac{^{40}\mathrm{Ar}^*}{^{40}\mathrm{K}}\right) \quad (5)$$

$$^{40}\mathrm{Ar}^* = \mathrm{K}\frac{^{40}\mathrm{K}}{\mathrm{K}}\frac{\lambda_e + \lambda'_e}{\lambda}(e^{\lambda t} - 1) \quad (6)$$

As S_{36Ca} is an effective total cross-section for the ^{36}Ar production from Ca for neutrons with a ^{235}U fission spectrum, the ^{40}Ca(n,nα)^{36}Ar$_{Ca}$ reaction can be expressed in eqn (7).

$$^{36}\mathrm{Ar_{Ca}} = \mathrm{S_{36Ca}Ca}\Phi \quad (7)$$

Eqn (8) can be formulated from dividing eqn (6) by eqn (7).

$$\frac{^{40}\mathrm{Ar}^*}{^{36}\mathrm{Ar_{Ca}}} = \frac{1}{\mathrm{S_{36Ca}}\Phi}\frac{\mathrm{K}}{\mathrm{Ca}}\frac{^{40}\mathrm{K}}{\mathrm{K}}\frac{\lambda_e + \lambda'_e}{\lambda}(e^{\lambda t} - 1) \quad (8)$$

Table 1 Summary of the average signals of different sample type analysis

	^{40}Ar analyzed by H2			^{36}Ar analyzed by L2		
Sample name	Average[a] (fA)	Uncertainty[b] (%)	SD[c] (%)	Average[a] (fA)	Uncertainty[b] (%)	SD[c] (%)
S0	15 321.65	0.01	0.21	51.22	0.08	0.20
S1	8394.86	0.01	0.36	28.07	0.13	0.36
S2	4478.67	0.01	0.12	14.96	0.22	0.23
S3	2401.50	0.01	0.23	7.98	0.41	0.47
S4	1291.44	0.01	0.28	4.27	0.76	0.87
S5	701.80	0.02	0.17	2.30	1.37	1.64
S6	382.83	0.03	0.15	1.25	2.45	2.22
S7	226.45	0.06	0.20	0.72	4.58	17.72
S8	135.23	0.17	0.75	0.43	6.93	16.85
BLK	30.45	0.31	2.55	0.05	54.81	64.6

[a] At least 20 times analysis for every type of sample were used to calculate the average, and no rejection. [b] Uncertainty (%): the average of the extrapolation result relative standard error. [c] SD (%) = stdeva(sample results)/average × 100.

When $^{40}Ar^*/^{36}Ar_{Ca} \geq 29\,856$, the maximum fast irradiation fluency can be calculated from eqn (9) for and any one t and K/Ca ratio. Thus, for a given K/Ca ratio, the accumulation fluence of fast neutrons is a function of t.

$$\Phi \leq \frac{1}{29856 \times S_{36Ca}} \frac{K}{Ca} \frac{^{40}K}{K} \frac{\lambda_e + \lambda'_e}{\lambda} (e^{\lambda t} - 1) \quad (9)$$

3.3. Sample size

The amount of sample should be chosen to ensure sufficient $^{40}Ar^*$ for the $^{40}Ar/^{39}Ar$ age spectrum to be measured with adequate resolution. The K–Ar dating computational formula (eqn (5)) can be used to estimate the sample size for typical sensitivity of individual mass spectrometry.

As the K isotopic composition in natural materials is essentially constant ($^{40}K = 0.01167\%$),[17] by substituting the potassium content, the abundance of ^{40}K and the quantity of matter in eqn (5), it can be rearranged into eqn (10) as follows:

$$W = \frac{M}{0.01167\alpha} \frac{\lambda}{\lambda_e + \lambda'_e} \frac{^{40}Ar^*}{e^{\lambda t} - 1} \quad (10)$$

where W = sample size in gram, α = K content in the sample and M = relative atomic mass of K (39.0983 g mol^{-1}). Thus, for a given α, W is a function of t.

4. Modified method to select accumulation fluence of fast neutrons

To estimate the detection limit of this analytical method, the analytical ability was evaluated through analytical uncertainty and external precision. Analytical uncertainty was evaluated as the relative standard error for samples S0–S8 extrapolated to time zero. The external precision was calculated from the spot-to-spot analysis for the same type of sample.

4.1. Analytical ability for 10^{11} Ω and 10^{12} Ω resistor Faraday cups

The Faraday cups of the H2 load with the 10^{11} Ω circuit and the L2 load with the 10^{12} Ω circuit were used to analyze ^{40}Ar and ^{36}Ar, respectively. Samples S0 to S8 were used to evaluate the analytical precision in the 10^{11} Ω and 10^{12} Ω resistor Faraday cups. The limit of detection (LOD) is evaluated to be six times the background signal. The average background signal of ^{40}Ar and ^{36}Ar is 30.45 fA and 0.05 fA, respectively. Thus, in our analytical system, the LOD is ~180 fA and 0.3 fA for ^{40}Ar and ^{36}Ar, respectively.

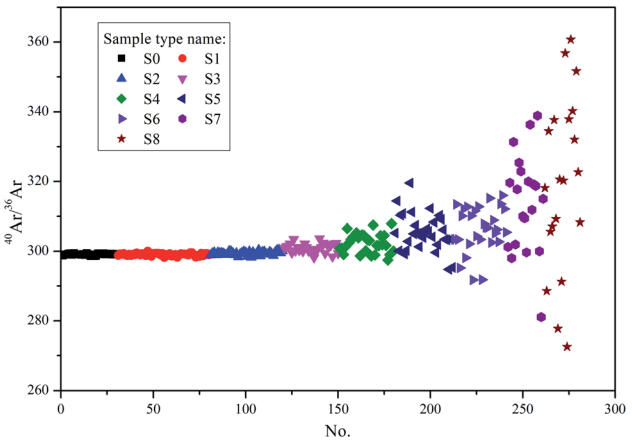

Fig. 3 Plot showing $^{40}Ar/^{39}Ar$ ratio with changes in different signal sizes.

During air argon isotopic analyses, a total of 7.66×10^{-13} mol of ^{40}Ar can yield an electric current signal of ~15 321 fA in the 10^{11} Ω circuit Faraday cup, with an analytical uncertainty of 0.009%. However measurements of sample S7 showed values approximately closer to the LOD and yielded an uncertainty of 0.06%. Furthermore, when the ^{40}Ar beams are lower than the LOD, the uncertainty increases rapidly (still <1%) with decreasing ion beam size (Fig. 2a). This phenomenon is also reported by a previous study,[4] which confirms no significant difference for analyzing ^{40}Ar signals from 230 000 fA to 1000 fA using the 10^{11} Ω circuit.

As for the 10^{12} Ω circuit, a beam intensity of 2.56×10^{-15} mol ^{36}Ar can yield ~51 fA electric current signal, and the analytical uncertainty is 0.076%. However, when decreasing the beam intensity to near the LOD (Sample S8), the average uncertainty is about 6.9%, which is much higher than 1%. Furthermore, it is noted that for the ^{36}Ar beams <~8 fA (uncertainty = 0.41%), the

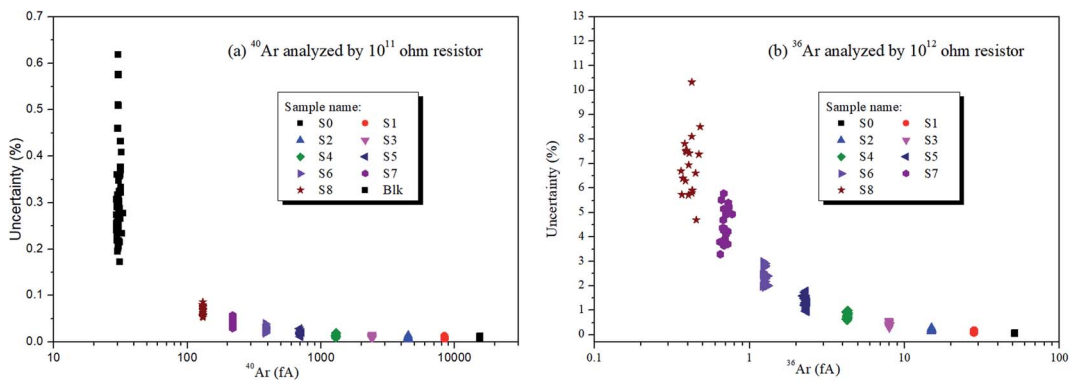

Fig. 2 Within-spot measured error *versus* signal intensity analyzed through the (a) 10^{11} Ω Faraday cup and (b) 10^{12} Ω Faraday cup.

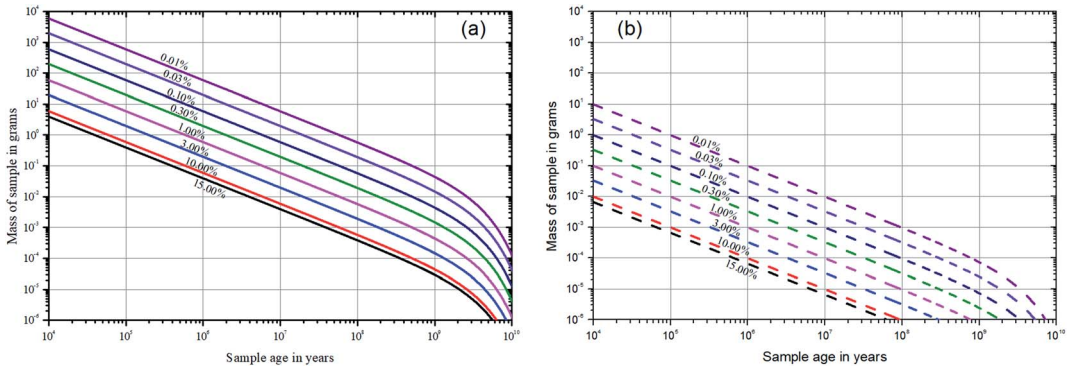

Fig. 4 Mass of the sample required to yield the precise result of $^{40}Ar^*$: (a) maximum and (b) minimum sample size for different K content samples. The value on the curves refer to the K content.

uncertainty increases rapidly with decreasing ion beam size (Fig. 2b).

Standard deviation (SD) for the $^{40}Ar/^{36}Ar$ ratio in spot-to-spot analysis increases from 0.08 to 7.78% as the ^{36}Ar signal decreases from 51 to 0.43 fA. It is noted that the SD of sample S4 ($^{40}Ar = 1200$ fA, $^{36}Ar = 4$ fA) reaches 0.91% and has significant variation (Table 1; Fig. 3). As the analytical uncertainty is governed by low-signal analysis, this may also limit the maximum $^{40}Ar/^{36}Ar$ ratio analyzed by Argus VI. When the beam intensity is higher than 8 fA (3.99×10^{-16} mol, sample S3), it can yield better than 1% analytical precision. Thus, ~8 fA is the acceptable lower limit for the 10^{12} Ω resistor Faraday cup, and can be used to estimate the maximum $^{40}Ar/^{39}Ar$ ratio.

4.2 Minimum sample size

The sensitivity of the Argus VI is about 7×10^{-14} mol V^{-1} at 200 μA trap current, which is significantly enhanced compared with that of conventional signal collector mass spectrometers.[4] With the help of laser step-heating and a mini efficient preparation system, the background can be substantially reduced.[5,6] Thus, the choice of sample size can have a wider range. We suggest that ~230 000 and ~400 fA are the maximum and minimum signals to yield ~1% analytical precision for the 10^{11} Ω circuit Faraday cup, which requires 9.51×10^{-12} mol and 1.65×10^{-13} mol $^{40}Ar^*$, respectively. Hypothetical the result needs 10 steps on the same amount of $^{40}Ar^*$, 9.51×10^{-11} mol $^{40}Ar^*$ and 1.65×10^{-12} mol $^{40}Ar^*$ are needed for the maximum and minimum signal, respectively. Thus, the optimum sample size range can be calculated with eqn (1), as shown in Fig. 4. When using ZBH-25 (132.7 Ma, K content: 7.597%) to estimate the suitable sample size, if ~230 000 fA and ~400 fA are the maximum and minimum ^{40}Ar signal intensities for each step (10 steps per sample), the maximum and minimum required sample sizes are 56 mg and 0.1 mg, respectively. When choosing the sample size in this range, the analytical precision of $^{40}Ar^*$ can be better than ~1%.

4.3. Maximum $^{40}Ar/^{39}Ar$ ratio

According to the above discussion, it can be assumed that the accurate analysis lower limit on the Faraday cup with the 10^{12} Ω circuit is 10 fA, and the maximum of the Faraday cup with the 10^{11} Ω circuit is 460 000 fA. Thus, the maximum of the $^{40}Ar/^{39}Ar$ ratio will reach 46 000. Even considering half of the signal of $^{40}Ar^*$ (~230 000 fA) and double the signal of ^{39}Ar (~20 fA) to yield more precise results, the $^{40}Ar^*/^{39}Ar_K$ ratio can reach 11 500. Furthermore, if the ^{39}Ar signal is fourfold the lower limit, the signal is 40 fA, or if the $^{40}Ar^*$ signal reached a quarter of the maximum value (~115 000 fA), the $^{40}Ar^*/^{39}Ar_K$ ratio would reach 5750.

According to eqn (4), the J value is a time function. When the acceptable $^{40}Ar^*/^{39}Ar_K$ ratio increases significantly from 300 to 5750 or 11 500, the accumulation fluence of fast neutrons can be largely decreased. Based on the above estimation and the conventional optimal estimate, we set the $^{40}Ar^*/^{39}Ar_K$ ratio to 1000, 5750, and 11 500 for the calculations. The boundary for different $^{40}Ar^*/^{39}Ar$ ratios can be calculated and upgraded using the Grenville Turner[3] plot as shown in Fig. 5. This modified plot

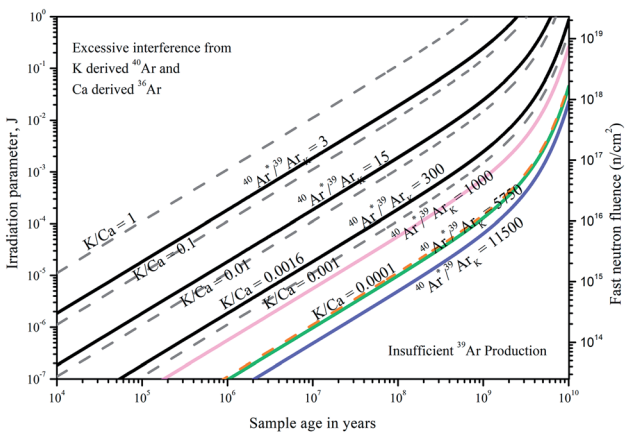

Fig. 5 Diagram showing the irradiation parameter modified from that described by Grenville Turner.[3] The dashed curves show the function of the maximum accumulation fluence of fast neutrons and the sample age (in year) at different K/Ca ratios and this study extends the ratio from 0.001 to 0.0001 (orange dashed curve). The pink, green, and blue curves show the minimum sufficient ^{39}Ar production that occurs for the accumulation fluence of fast neutrons, estimated here for $^{40}Ar^*/^{39}Ar = 1000$, 5750, and 11 500, respectively.

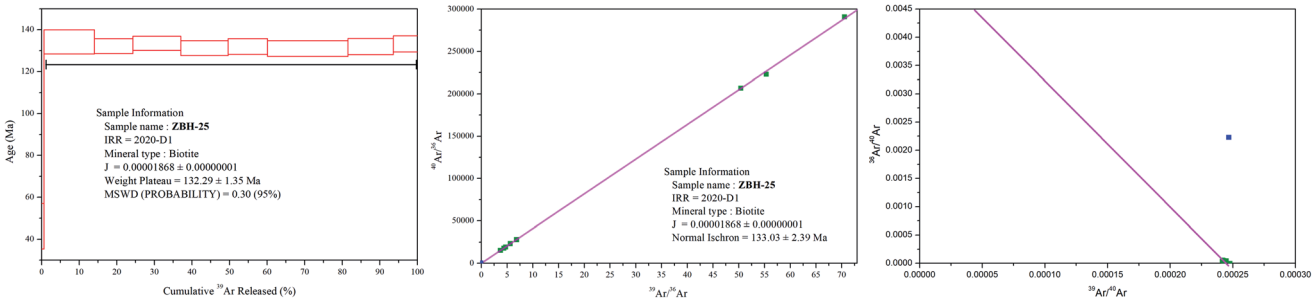

Fig. 6 $^{40}Ar/^{39}Ar$ age spectrum, normal isochron, and inverse isochron for ZBH-25 by laser step-wise heating.

Table 2 $^{40}Ar/^{39}Ar$ dating results for ZBH-25

Step	Laser power (W)	$^{36}Ar(a)$ (fA)	$^{37}Ar(Ca)$ (fA)	$^{38}Ar(Cl)$ (fA)	$^{39}Ar(K)$ (fA)	$^{40}A(r)$ (fA)	Age (Ma)	±2 s	$^{40}Ar(r)$ (%)	$^{39}Ar(K)$ (%)	K/Ca	±2 s	$^{40}Ar(r)/^{39}Ar(K)$
S01	5.5%	6.06	0.07	0.03	0.67	928.87	46.19	±10.84	34.16	0.60	5.2	±6.6	1384.5
S02	16.0%	0.21	0.51	1.64	15.07	62 144.34	134.20	±5.75	99.90	13.41	16.7	±3.9	4122.6
S03	16.0%	1.69	0.12	0.19	11.55	46 885.05	132.18	±3.54	98.94	10.28	54.3	±37.8	4058.4
S04	20.0%	0.28	0.14	0.75	14.28	58 569.05	133.51	±3.44	99.86	12.71	56.3	±38.6	4100.5
S05	24.0%	0.26	0.16	0.83	14.18	57 124.87	131.23	±3.53	99.87	12.62	50.1	±31.0	4028.0
S06	28.0%	3.18	0.18	0.14	11.72	47 488.80	132.01	±3.76	98.06	10.43	36.9	±17.5	4052.7
S07	33.0%	5.14	0.32	0.41	24.12	96 966.34	131.01	±3.76	98.46	21.46	42.0	±15.3	4021.0
S08	39.0%	3.10	0.15	0.20	13.56	54 908.30	131.92	±3.88	98.36	12.06	51.5	±33.5	4050.2
S09	45.0%	1.28	0.12	0.27	7.22	29 545.59	133.26	±3.82	98.73	6.42	33.7	±26.3	4092.6

recommends a low K/Ca ratio of <0.001 to choose the accumulation fluence of fast neutrons.

If this boundary were the case, the accumulation fluence of fast neutrons can decrease one to two orders of magnitude compared to that conventionally recognized.[1] Moreover, reducing the irradiation fluence can minimize the nuclear reaction of $^{40}Ca(n,n\alpha)^{36}Ar$, especially for low-K/Ca samples. Thus, we recommend that the maximum $^{40}Ar^*/^{39}Ar_K$ to calculate the minimum fast neutron flux is 5750. This boundary can guide us to choose the irradiation parameters when the samples have K/Ca < 0.001.

5. Sample verification

Nine steps were run during laser step-wise heating, and the first step exhibiting a slightly irregular age plateau was excluded. Eight concordant steps were carried out. This released 99.40% of the total ^{39}Ar released, and gave a weighted mean plateau age of 132.29 ± 1.35 Ma (MSWD = 0.30) at the 95% confidence level in J = 0.00001868. These eight steps also yielded normal and inverse isochron ages of 133.03 ± 2.39 Ma (MSWD = 0.30) and 132.82 ± 2.38 Ma (MSWD = 0.30), respectively. All ages fall within the error of the recommended age.[7] The raw data, $^{40}Ar/^{39}Ar$ age spectra, and isochron plots (normal and inverse) are presented in the Appendix.

The age spectra and isochron plots are shown in Fig. 6. The $^{40}Ar^*/^{39}Ar$ ratios of these eight steps range from 4020 to 4122, and details of $^{40}Ar/^{39}Ar$ age data are shown in Table 2. When calculate the accumulation fast neutron fluence, it also coincides with the theoretical calculated value through the reactor parameters. This also shows that when $^{40}Ar^*/^{39}Ar$ reaches ~4100, the analytical precision obtained can be better than ~1%, which in turn suggests that our above calculations and modified boundary are practical.

6. Conclusions

Theoretically, the $^{40}Ar^*/^{39}Ar$ ratio up to 5750 can still yield ~1% analytical precision on an Argus VI noble gas mass spectrometer in GIGCAS. Moreover, the observation that ZBH-25 irradiated for 4 h yielded a higher $^{40}Ar^*/^{39}Ar$ ratio (up to ~4100) in the samples has verified this theoretical calculation. This indicates that a $\sim 10^{15}$ n cm^{-2} accumulation fluence of fast neutrons can be selected for sample irradiation, which is three orders of magnitude below what was previously recognized. This modified boundary can help to choose the accumulation fast neutrons fluence during irradiation, especially for very old or low-K/Ca samples.

Author contributions

W.-F. Z. and D.-W. Z. jointly designed the paper. W.-F. Z. wrote the main text. D.-W. Z. and Y.-G. X. revised it critically for important intellectual content. W.-F. Z. and G.-Q. L. performed sample irradiation. And W.-F. Z. and Y.-D. J. performed the analytical work and provided interpretations.

Conflicts of interest

There are no conflicts to declare.

Acknowledgements

This study was financially supported by the Key Special Project for Introduced Talents Team of Southern Marine Science and Engineering Guangdong Laboratory (Guangzhou) (GML2019ZD0202), the Guangdong Basic and Applied Basic Research Foundation (No. 2019A1515012190), the National Natural Science Foundation of China (No. 41603045) and GIG-CAS (GIG-GNKF-202002). A Guangdong Special Support Program for Y. D. Jiang is also acknowledged. This is contribution No. IS-3021 from GIGCAS.

References

1 I. McDougall and T. M. Harrison, *Geochronology and thermochronology by the $^{40}Ar/^{39}Ar$ method*, Oxford University Press, New York, 1988.
2 D. Phillips, E. L. Matchan, M. Honda and K. F. Kuiper, *Geochim. Cosmochim. Acta*, 2017, **196**, 351–369.
3 G. Turner, *Earth Planet. Sci. Lett.*, 1971, **10**, 227.
4 D. F. Mark, D. Barfod, F. M. Stuart and J. Imlach, *Geochem., Geophys., Geosyst.*, 2009, **10**, Q2A.
5 X. J. Bai, H. N. Qiu, W. G. Liu and L. F. Mei, *J. Earth Sci.*, 2018, **29**, 408–415.
6 W. F. Zhang, H. N. Qiu, D. W. Zheng, Y. D. Jiang and X. J. Bai, *Geochimica*, 2020, **49**, 509–515.
7 S. S. Wang, *Sci. Geol. Sin.*, 1983, 315–323.
8 J. Lee, K. Marti, J. P. Severinghaus, K. Kawamura, H. Yoo, J. B. Lee and J. S. Kim, *Geochim. Cosmochim. Acta*, 2006, **70**, 4507–4512.
9 A. Koppers, *Comput. Geosci.*, 2002, **28**, 605–619.
10 A. J. Schaen, B. R. Jicha, K. V. Hodges, P. Vermeesch, M. E. Stelten, C. M. Mercer, D. Phillips, T. A. Rivera, F. Jourdan, E. L. Matchan, S. R. Hemming, L. E. Morgan, S. P. Kelley, W. S. Cassata, M. T. Heizler, P. M. Vasconcelos, J. A. Benowitz, A. A. P. Koppers, D. F. Mark, E. M. Niespolo, C. J. Sprain, W. E. Hames, K. F. Kuiper, B. D. Turrin, P. R. Renne, J. Ross, S. Nomade, H. Guillou, L. Webb, B. A. Cohen, A. T. Calvert, N. Joyce, M. Ganerød, J. Wijbrans, O. Ishizuka, H. Y. He, A. Ramirez, J. A. Pfänder, M. Lopez-Martínez, H. N. Qiu and B. S. Singer, *Geol. Soc. Am. Bull.*, 2020, **133**(3–4), 461–487.
11 C. Merrihue and G. Turner, *J. Geophys. Res.*, 1966, **71**, 2852–2857.
12 R. L. Crasty and J. G. Mitchell, *Earth Planet. Sci. Lett.*, 1966, **1**, 121–122.
13 P. R. Renne, R. Mundil, G. Balco, K. Min and K. R. Ludwig, *Geochim. Cosmochim. Acta*, 2010, **74**, 5349–5367.
14 R. H. Steiger and E. Jäger, *Earth Planet. Sci. Lett.*, 1977, **36**, 359–362.
15 J. G. Mitchell, *Geochim. Cosmochim. Acta*, 1968, **32**, 781–790.
16 L. T. Aldrich and A. O. Nier, *Phys. Rev. A: At., Mol., Opt. Phys.*, 1948, **47**, 876–877.
17 E. L. Garner, T. J. Murphy, J. W. Gramlich, P. J. Paulsen and I. L. Barnes, *J. Res. Natl. Bur. Stand., Sect. A*, 1975, **79**, 713–725.

